J. Condensed Matter Nucl. Sci. 23 (2017) 91–116

Research Article

Perspective on Low Energy Bethe Nuclear Fusion Reactor with Quantum Electronic Atomic Rearrangement of Carbon

Stephane Neuville*

TCE Consulting, F-77165, Cuisy, France

Abstract

The relatively low/medium proton/carbon collision threshold energy (1–8 keV) of the Bethe–Weizsäcker nuclear reaction cycle C, N, and O observed in low temperature carbon rich stars suggests the eventual technical feasibility of a solid-state carbon fusion reactor. H^+ used as a precursor nuclear material can be implanted in solid-state carbon material. We must then consider all effects that can affect nuclear collision efficiency, including solid-state structure specificity, proton channeling and the reduction of the original proton energy with electronic interactions, before looking at the possible nuclear reactions themselves. We then have to consider the different effects and types of atomic rearrangement favoring either sp2 or sp3 sites or which influence the carbon material structure. For this purpose, we review first a recently developed theoretical approach, which might explain important aspects of this phenomenon with still high confidence up to now. These aspects include quantum electronic activation especially with H_2 recombination energy release, which is different from usual chemical and metallurgical thermal atomic rearrangement with which an optimized ta-C sp3 carbon structure can be controlled. It should also be considered that carbon structure determination methodology – including the recently revised Raman theory – provide more correct and accurate results. To be falsified a study of this type of proton–carbon nuclear reactor must also take into account effects which modify the carbon nucleus structure in favor of nuclear fusion. It is suggested that anharmonic synchronic phonon–nuclear resonance may be a contributing factor. However, present failures and the limits of abstract Quantum Mechanical formalism bring little clarification on this last point, which we suggest is owing to insufficient physical description of particle wave character. In order to improve these aspects of the theory, we suggest revisiting aether theory which with further investigation and development of 3D fluid mechanics is expected to account for all QM acquired, and to be able to provide clearer physical insight into the subatomic particle wave aspects and corresponding nuclear reaction mechanism.
 ISSN 2227-3123

Keywords: Anharmonic phonon–nuclear resonance, Bethe–Weizsäcker proton CNO fusion reactor, Carbon material characterization, Synchronic phonon/proton–nucleus collision, Quantum electronic atomic rearrangement

*E-mail: stephane.neuville709@orange.fr; Tel.: +33 (0)6 4147 1922.

© 2017 ISCMNS. All rights reserved. ISSN 2227-3123

1. Introduction

Nuclear fusion reactions involving hydrogen isotopes have been the subject of many investigations with magnetic and inertial hot plasma fusion devices [1,2], in particular with compact high voltage (∼100 keV) electric discharge D–D fusion neutron generators [3–5]. Such studies have also been made with nuclear fusion in solid state material. This technique may avoid the production of long lived radioactive waste, and it is expected to have higher energy production capability than nuclear fission [6,7].

Considering the relatively low threshold collision energy (1 keV range) of a nuclear fusion reaction of the Bethe–Weizsäcker H+/C, N, and O fusion cycle (Table 1), and the relatively reduced amount of energetic secondary emission [8], we focus on the study of eventual technical feasibility of a hybrid plasma/solid state H^+/carbon fusion reactor.

Cold plasma devices are used for sputtering and Plasma Assisted Chemical Vapor Deposition (PACVD) and Arc deposition. Some of the common ones have ion energy in the 1 keV range and plasma density in pulsed mode up to 10^{12} ion/cm^3 and which can produce substrate ion current density up to about 100 mA/cm^2 [9–19]. Dense cold plasma hydrogen in the 1 kW discharge power range (for instance with a plasma reactor of ∼50 cm size) can produce $\sim 10^{19}$ p+/s in a 1 keV range which can interact with a carbon target material surface with 10^{15} a/cm^2 and with ion implantation depth of ∼1000 atomic layers. This corresponds to solid state volume containing $\sim 10^{21}$ carbon atoms which can interact with impinging protons (considering for instance 100 μs DC pulsed mode with 10 ms duty cycle) [20–22].

The reported proton nuclear reaction rate is about 10^{-3} [7] achieved with a picosecond high energy proton source [23]. This produces a laser shot generated proton bunch, containing $\sim 10^7$ protons of energy above the nuclear collision fusion threshold. This collides with a dense boron plasma estimated in the 10^{16} ion/cm^3 range (produced by a 1 ns laser shot after 1 ns expansion [7]). Considering the size of the roughly described cold plasma/carbon solid state reactor described above, and the proton nuclear reaction rates analogous to the previously mentioned proton/boron plasma experiment, this would correspond to a theoretical delivered nuclear power of ∼100 kW.

No fusion energy has been reported with diamond-like carbon (DLC) cladded hot plasma reactor wall. These reactor walls are used in order to avoid erosion of refractory heavy metal wall material [24,25]. We suggest this can be explained to some extent by the much lower p+ flux on the reactor wall. The same explanation may also apply to a thermal shield solar wind erosion study [26,27].

However, with an experiment using simulated solar wind 2 keV/4 keV proton irradiation (in the 10^{-8} A/cm^2 range) of a carbonaceous target [26,27], the following was observed: with recently revisited Raman spectroscopy fundamentals [28] and detailed analysis of Raman spectrum, it appears that the carbon material is subject to partial sp3 atomic rearrangement (an endothermic process) [29], which is enhanced with additional hard UV irradiation. This effect is normally not observed when a graphitic material for which the graphite crystallite are growing in size [30,31] is only heated, without hard UV irradiation.

From fusion experiments involving the collision of energetic H^+ flux on a dense boron plasma, it is known that fusion efficiency is much higher than for the same H^+ flux impinging on a solid-state boron target, which has paradoxically at least about $10^2/10^3$ much higher density of nuclei [7]. We suggest this should be interpreted with reference to

Table 1. Bethe CNO fusion cycle.

$^{12}C + ^1H$	→	$^{13}N + \gamma$ +1.95 MeV
^{13}N	→	$^{13}C + e^+ + \nu e$ +2.22 MeV
$^{13}C + ^1H$	→	$^{14}N + \gamma$ +7.54 MeV
$^{14}N + ^1H$	→	$^{15}O + \gamma$ +7.35 MeV
^{15}O	→	$^{15}N + e^+ + \nu e$ +2.75 MeV
$^{15}N + ^1H$	→	$^{12}C + ^4He$ +4.96 MeV

the fact that H^+ loses in a solid-state material ($\sim 10^{22}$ atom/cm^3) about 90% of its energy with electronic interaction [25]. Only a reduced amount of implanted H^+ will have energy above nuclear reaction threshold and can collide with carbon nuclei. Meanwhile, the optimized nuclear collision probability is achieved with much lower electron density ($<10^{16}$/cm^3) in an expanding plasma, according to an experiment produced with high energy proton interacting with such expanding plasma [7, 21,22]. Thus, showing the importance of (a) electronic shielding which has to be kept as low as possible and (b) reduced H^+ channeling with which H^+ can lose much of its energy before colliding with a carbon nucleus. This is a particularly important effect in crystalline carbon material and especially in diamond [32–40]. These results suggest that the carbon material should be as dense as possible, and amorphous.

The question is then whether the resulting distribution of collision density and energy in carbon materials might be sufficient to cause a significant amount of nuclear reactions producing more energy than consumed. Therefore, the first thing to consider is whether different physicochemical effects which affect the atomic distribution of atomic nuclei and the resulting atomic structure which determines the electronic spatial distribution of each nucleus.

Beside evaporation/sputtering of the carbon target, it is especially important to consider the role of atomic rearrangement induced by quantum electronic activation (QEA) (reviewed in Section 3) [29]. Evidence for this effect was first seen in carbon materials, considering the important differences of carbon material properties linked to its structure [41] and based on different electronic orbital hybridization (mainly sp2 and sp3), different atomic packing density and different interatomic bond energy [9]. However, it is only possible to conveniently observe this with detailed and accurate characterization of carbon material structure for which updated Raman spectrometry fundamentals appears necessary [28]. This is the reason we include a brief review in Section 4.

Although no Mossbauer effect can be observed with carbon atoms (essentially a question of the misfit between available γ source wave length and nuclear energy levels) [42,43] some modification – however small – of its nuclear structure under the influence of the electronic environment is to be expected, which might affect the fusion collision energy threshold with some synchronic mechanisms. We will discuss this in Section 5.

It appears that conventional quantum mechanical formalism at the present stage cannot explain all aspects of electron/nucleus interaction which might enhance nuclear reaction efficiency. In order to get clearer insight on how nuclei can be fused after collision we suggest revisiting some aspects of quantum mechanics (discussed in Section 6).

2. Hydrogen in Materials

Hydrogen being monovalent, bonding chain discontinuities can appear. If chemically bonded on one side (M–H…, then the H atom will generally be only weakly bonded on the other side. Instead of strong M–M–M chains, it will be possible to have weak M...H–H...M chains able to enhance some of the brittleness of metals [44]. This explains the lower hardness and plasticity of polymers [9,45]. Hydrogen is more easily introduced in substrate material which has lower atomic density and especially after being dissociated to H* and/or ionized to H^+. And this effect is clearly shown with results of ion implantation and H^+ channeling experiments [20,34–40,46]. The H* and H^+ hydrogen can be absorbed in higher amounts in more porous and less dense metals [47,48].

The reverse effect is likely to be achieved when the material is heated up with H_2exodiffusion, when M–H binding energy is lower than H–H ($\sim$5 eV and a similar level for O–H) in comparison for instance to C–H ($\sim$4 eV up to 4.5 eV) and to H…H physical hydrogen bonds ($\sim$0.1 eV). This explains, for instance, the relatively reduced thermal and chemical stability of polymeric carbon material and their reduced hardness, whenever they contain a high number of sp3 sites such as in diamond [9,29]. Frozen methane containing 100% sp3 has nothing to do with diamond and has, like frozen water, only relatively low hardness compared to harder steel, chromium, Al_2O_3, CW, TiN, etc. (hardness density of cohesion energy [29,48]). H can also be more tightly trapped in denser and harder materials corresponding to good diffusion barrier properties for H_2, such as ta-C and defect-free graphene and also glassy carbon, the latter despite being porous (with isolated pores) [49,50], in contrast to H^+ for which even graphene is porous [51]. Therefore,

trapped atomic hydrogen released with the higher temperature can recombine to H_2 with Chemical Recombination Energy Release (CRER). This energy can be partly absorbed with anomal atomic rearrangement, before being released in the form of heat [52].

This has been observed especially with Nickel alloys [53], and miscellaneous other alloys [54,55] for which hydrogen is introduced in the bulk through the surface by different means (for instance with H^+ in a polarized salty solution, or when H_2 is dissociated on the surface by catalytic effects, or with plasma surface interaction producing ion implantation, etc.). In such cases, after the exodiffusion of recombined H_2, tensile stress and cracks can appear favoring brittleness whenever no hydrides have been formed [56]. Therefore, atomic rearrangement to a structure with higher atomic packing density where the endothermic intrinsic atomic rearrangement effect can be in competition with the exothermic effect of the chemical recombination energy release, as we briefly review in Section 3.

3. Brief Review of Quantum Electronic Atomic Rearrangement

Many experiments in the chemical synthesis and formation of metastable material have shown that quantum electronic activation effects obtained, for instance with various photonic excitations, can play a decisive role for the achievement of some desired specific molecular configuration, and that it is not possible to replace photon activation by equivalent heat introduced from outside [57].

Quantum electronic atomic rearrangement (QEAR) for which higher activation energy (1–10 eV range) is involved, is different from Thermal Solid-State Atomic Rearrangement (TAR) where much lower thermal energy is generally involved (0.01–0.3 eV range) corresponding to temperature lower than 3000 K. The QEAR can be caused by many different kinds of physical electronic activation (before being transformed into heat) and therefore often produces metastable structures, whenever the effect is also able to enhance transformation kinetic towards ground state (for instance Si recrystallization either with H_2 recombination or by laser processing) [58–60]. Meanwhile TAR is ruled by Arrhenius thermal statistics which generally transforms the material towards its groundstate and which can be in competition with the first effect. Higher activation energy levels and rates can produce atomic rearrangement of merely graphitic material towards a harder and denser diamond-like carbon structure, meanwhile temperature will convert glassy carbon, diamond-like carbon and diamond to graphite [29,31,61,62].

Many other materials, including different metals, are known to have different oxidation states corresponding to different stoichiometric possibilities and atomic structures of different atomic packing density, such as C, Cr, Fe, Ni, Cu, Pd, Ta, etc. [44,48,63], and for which different hybridization states can exist, generally corresponding to hexagonal and cubic structure of different packing density [64]. For instance, cubic Si corresponds to its ground state, while silicene corresponds to a metastable structure [65], in contrast to carbon and to nickel.

Given the numerous compounds associated with different carbon solid state configurations between monocrystalline diamond and monocrystalline graphite [41,66] (Fig. 1), different kinds of atomic rearrangement exist [29], which can be detected by the modification of the carbon solid state optoelectronic gap (which is much higher in diamond and diamond like material than in graphitic material), and with accurate characterization of the different carbon types [9,67]. Raman spectrometry is considered one of best carbon characterizion tools. However, many incoherent aspects of this technique could be found in literature. This is why the latest updated method has to be used in this study [28], as we briefly explain in Section 4.

3.1. Graphitic thermal degradation and metastable diamond-like material reforming

Graphitic degradation is generally observed during longer thermal annealing of diamond [31,61,68]. This produces different kinds of diamond-like carbon (DLC) [41,61], including the so-called amorphous hydrogenated carbon (a-C:H) [52] and carbon material such as filled carbon wires and fibers containing both sp2 and sp3 sites [69,70]. Some

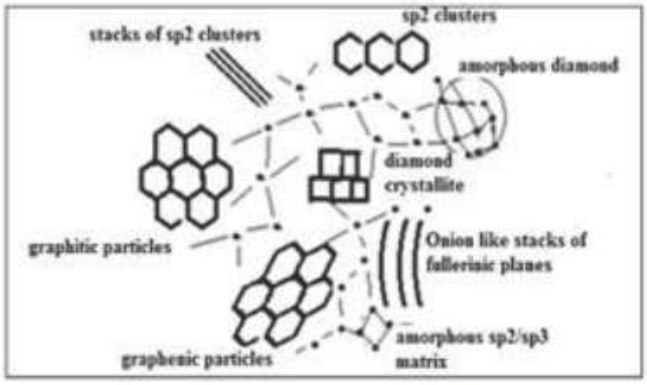

Figure 1. Scheme of composite DLC carbon material.

materials such as hollow carbon nano-tubes (CNT) or graphene, which are materials close to graphitic ground state (containing hexagonal cyclic rings similar to graphite), will not be degraded and can have some defects eliminated at higher temperatures when the temperatures stay below sublimation temperature (∼3500 K) [71,72].

It is known that diamond, a metastable material, is formed when higher temperatures along with pressure, and that its thermal graphitic degradation starts at about 800° C [31,61,62], when no other physical effects hamper or go against this process [52,57,73,74]. This is the reason why some DLC material has been produced with thermal spikes during plasma and ionic processes [62]. However, many other effects other than pressure and thermal spikes have also been identified as favoring diamond-like materials and diamond growth, such as hot filament diamond deposition, low bias plasma deposition [68], energetic UV (>5 eV) [73], X-ray irradiation [75], chemical and catalytic reactions and especially those associated to H_2 and N_2 chemical recombination [29,52,67,76,77]. External input of heat alone will not produce diamond-like atomic rearrangement [57]. The Ion Beam Assisted Depositing (IBAD) process and Filtered Cathodic Vacuum Arc (FCVA) devices can produce ta-C when the density of the ion bombardment is high enough and when the temperature is low enough [10,11,78,79]. This is achieved with quantum electronic activation with released ion neutralization energy and ion implantation compressive stress which favor DLC with higher sp3 content and with the combination/addition of all these different effects [10,29].

With updated Raman spectroscopy [28] (reviewed in Section 3.2) many published works show that carbon material processing that is supposed to produce graphitic material, often in fact contains some DLC and sometimes also some nanocrystalline diamond [52,67]. This is shown, for instance, with graphitic material simultaneously heated up to 3000 K and irradiated with intense hard UV and 8 keV H+ [26,27], and with a glassy carbon corresponding to graphenic and fullerenic material containing sp3 with somewhat diamond-like (hardness ∼15 GPa) [49], for which a D diamond peak is observed at ∼1325 cm^{-1} [49,69] indicating the existence of H6 hexagonal chair diamond structure [31,79,80]. Meanwhile in this case, only a weak (∼10 times lower intensity than H6 peak) the so-called D-disorder band at ~ 1350 cm^{-1} is observed corresponding to GeA-edge phonon modes (in accordance to its overmode at ∼2700 cm^{-1} [28,29] of similar intensity).

3.2. Role of an electric field on diamond-like rearrangement of graphitic materials

An electric field is known to produce molecule distortion and polarization, which can initiate atomic rearrangements, when the polarizing energy E_{p} is higher than some threshold energy [29].

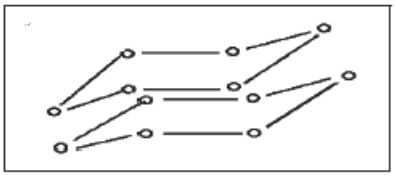

Figure 2. Stack of chair shape hexagonal cyclic rings corresponding to H6 diamond structure with sp3 sites (one carbon atom bonded equivalently to four others). Raman frequency at $\sim$1325 cm^{-1} according to Spear et al. [81] and Huong et al. [31].

Especially hexagonal cyclic sp2 ring can be transformed into hexagonal sp3 chair structure [28,29], an observed effect when applying an electric field on aromatic compounds [82] and which can transform graphitic materials into diamond-like materials containing sp3 [83].

Consider a stack of graphene hexagonal sp2 rings, in graphite and in a multiwall carbon nanotube. These can be transformed into stack of chair shape sp3 hexagonal ring [29,31,81] (Fig. 2) corresponding to H6 diamond. This is an intermediary structure between graphite and diamond, which can be observed, for instance, on the external surface of carbon fibers and wires containing both sp2 and sp3, when produced with plasma activation [69,70]. A H6 structure can also be obtained by thermal graphenic degradation of carbon deposited on a cubic Si substrate, or with the epitaxial growth of Si on a graphene substrate forming a non-planar buckled silicene layer [65]. Then consider how a transient electric field can be produced in a growing carbon material film, with the different reported activation mechanisms favoring DLC material growth. Adsorption of molecules on some semiconducting materials can produce a transient transverse electric field, similar to what is achieved with the Dember effect [84]. This occurs when pairs of electron/hole (with different diffusion mobility) are activated on a semiconductor surface, before producing heat and therefore, it is not of thermal origin. This happens instead via a direct transfer of adsorbtion energy to valence band electrons [29]. Investigation on CO adsorbtion on a Ni substrate confirm this effect by showing IR photon emission corresponding to the same adsorbtion energy release (no substrate heating) [85]

3.3. Role of released chemical recombination energy on valence band electron excitation

Energy released by electric neutralization ($\sim$10 eV), chemical recombination (CRER) ($\sim$1 up to $\sim$20 eV) and chemisorption ($\sim$7 eV in the case of C–C bond formation on appropriate surface sites) produces quite high activation energy, before it produces heat. H–H ($\sim$5 eV) recombination should mainly be considered, besides other types of high CRER such as O–H, F–H, etc. These are reviewed in [29]. Dissociation energy has to be subtracted from these.

Table 2 gives a list of recombination energy releases involving C and H during the growth of diamond and a-C:H with hydrocarbon precursors. Figure 3 shows how CRER is particularly important with chemical recombination of N$\equiv$N ($\sim$12 eV) and corresponding to many observable diamond crystallites which have been formed by atomic rearrangement during annealing of CNx materials and depending on N distribution [29,66]. A similar effect occurs with N+ ion bombardment where N can recombine to N2 with which glassy carbon can be transformed into N doped ta-C [87].

3.4. Criterion of quantum electronic sp3 activation

Carbon material has to be considered as semiconducting material (Fig. 4.), whenever the species are semimetals such as graphite and metallic nanotubes and with overlapping electronic valence σ/π and conduction σ^*/π^* bands [88].

Considering that during atomic rearrangement, the outer electron orbital activated electrons should always occupy

Table 2. H_2 and C–C chemical recombination energy release during hard carbon film growth with HC precursors.

a-C:H H* + H*	→	H_2 + (∼5 eV)	(F1)
Csp3-H + Csp3-H	→	Csp3 - Csp3 + H_2 + (∼3 eV)	(F2)
Csp3 -H + H*	→	Csp3 - Csp2 + H_2 + (∼0.5 eV)	(F3)
Csp3 <+ 2 H*	→	Csp2 + $2H_2$ + (∼1.5 eV)	(F4)
Csp3 <+ 2 H*	→	Csp2 + $2H_2$ + (∼1.5 eV)	(F5)
Csp2 <+ Csp2 <	→	Csp2 - Csp2 + $2H_2$ + (∼1 eV)	(F6)
Csp2 <+ Csp3 <	→	Csp2 - Csp3 + $2H_2$ + (∼1 eV)	(F7)
Csp3 <+ Csp3 <	→	Csp3 - Csp3 + $2H_2$ + (∼1 eV)	(F8)
(with C<representing CH2)			

authorized energy levels, we postulate that they should be always activated to energy levels higher than both the original and final state (Fig. 5).

However, other conditions also have to be fulfilled. The number of activated electrons should be higher than the number of atoms which can be rearranged. This is a five-dimensional phenomenon involving local space, energy and time and for which simultaneity, activation energy level, activation intensity and the decay of several valence band electron activation events must be compatible with steric aspects. Some equations of atomic rearrangement have been established illustrating all aspects to consider [29], but we will not reproduce these equations in this review.

Carbon material can have an optoelectronic gap from a very low value (<0.1 eV in graphenic materials) up to (∼2.5/3.5 eV) for DLC/ta-C and ∼5.2 eV for diamond. The rearrangement criterion applies also to carbon materials with a lower final gap for which lower activation energy will be sufficient (subject to enough electrons that are locally activated).

Diamond can be produced at higher temperature (T>1200 K), for which only graphitic soot would be expected if only considering usual thermal atomic rearrangement (which is governed by the Arrhenius law). Intense hydrogen CRER that favors sp3 activation can compensate for thermal graphitic degradation [29]. Longer high temperature thermal annealing of a-C:H, a-C, ta-C and diamond induces growth of sp2 clusters [31,52,73,74, 89]. However, shorter thermal treatment of a-C:H, can maintain or improve their diamond-like character for a while before being degraded with longer annealing time [58,63,77]. Heating up some polymers can produce a harder glassy carbon [49].

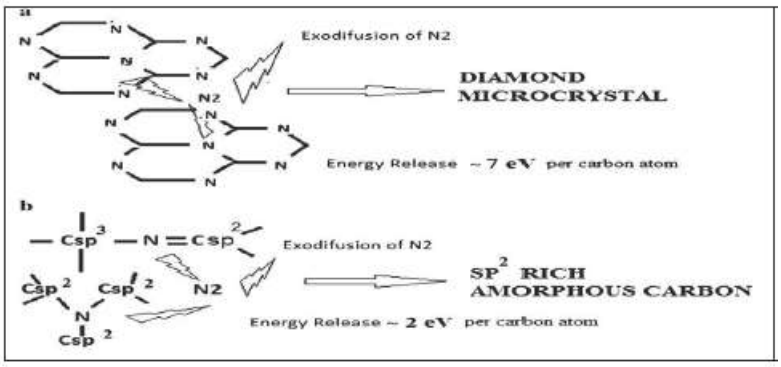

Figure 3. Formation of diamond crystallites with annealing (∼ 700° C) of CNx containing no molecular N_2 and ordered densely packed hexagonal planes containing substitutional H [29,66]. This is a controversial result considering that CNx annealing usually produces graphitic carbon when containing merely molecular N_2 content (few CRER) [9,86].

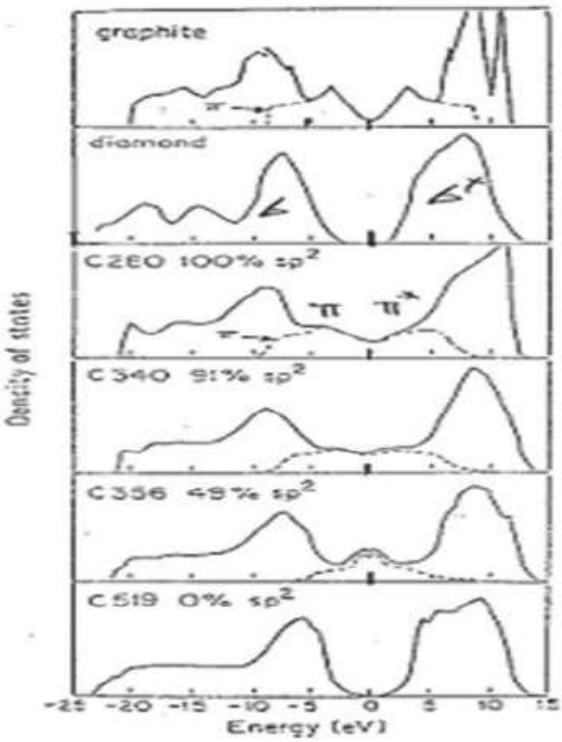

Figure 4. Density of electronic states in diamond, graphite, GLC, DLC and ta-C by Beeman et al. [76]. (1) Valence band electrons in graphite, GLC and DLC can be activated *by thermal activation* because of the reduced optoelectronic gap and low energy transition $\pi \rightarrow \pi^*$. (2) Whereas, for diamond and ta-C no significant $\pi\pi^*$ band exists (more or less only $\sigma\sigma^*$bands) and gap >3 eV has to be considered for which electron excitation *needs a higher quantum electronic activation.* (3) A continuous band allows reduced thermal activation in favor of graphitic degradation (with which Raman effect appears with laser excitation at 514 nm (2.41 eV) < gap.

3.5. Influence of atomic rearrangements on disorder and stress

Stress reduction is of particular importance because stress affects carbon film adherence [9,90,91]. Ordinary thermal annealing, while also relaxing stress, generally produces graphitic degradation. Therefore, another way to reduce stress without graphitic degradation has to be sought. Stress in carbon material can be determined by measuring mechanical bending of a thin substrate coated with the stressed material (reviewed in [9]), or by measuring the Raman shift [28,90]. Most ionic depositing processes generate internal compressive stress [91], while exodiffusion of hydrocarbon and H_2 can relax them and can sometimes produce tensile stress, when more important denser atomic rearrangement is to be considered [9,52].

Atomic rearrangements generally lead to internal stress reduction by reducing the number of defects (vacancies and interstitials) with which higher final atomic packing density and better ordered material can be achieved [28,29,76,77,86,92]. Stress can be reduced with carbon material sp3 restructuration by using electric field [83] or with thermal annealing when combined to high energy (>5 eV) such as with UV laser irradiation or X-ray irradiation [73,75].

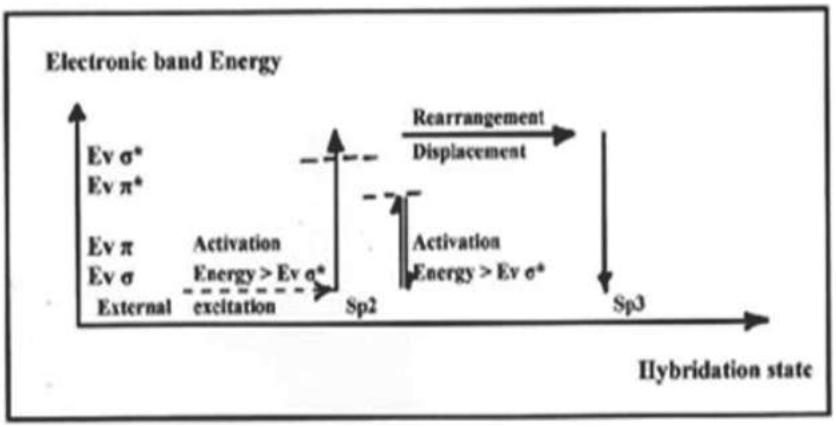

Figure 5. Sp3 rearrangement activation criteria [29]. During atomic rearrangement, electrons of the outer atomic shells must always occupy authorized energy levels. ⇒ valence electrons have to be excited up to conduction band levels of *initial and final* state before decay into the final valence band level.

3.6. Examples of application of sp3 rearrangement effects

3.6.1. *Catalytic effects*

Sp3 atomic rearrangements can be enhanced with catalytic effects which produce higher hardness and lower hydrogen content (exodiffusion). Considering that boron has similar bonding energy with H and C, reducing the original C–H bond energy and enhancing C–C and H–H recombination higher deposition rates and higher hardness and diamond-like quality of growing a-C:H and diamond can be achieved [9,29,76,77,92]. During the growth of an ordered diamond, only thermal stress is generally produced in consequence of a different thermal dilatation coefficient between the substrate material and coating [68].

3.6.2. *Transformation of graphene into the so-called graphane and related materials, when either atomic H* or N* or O* is adsorbed on a multilayer graphene surface*

This process transforms a highly electrical conducting graphene into a non-conducting diamond-like dielectric (gap ∼5 eV) [93,94]. We suggest this interpretation is questionable, and it is more likely explained by the transformation of graphene into an H6 material, which like silicene is not a planar structure (hexagonal buckled sp3 chair structure). A sharp Raman peak appears in a Raman frequency range of ∼1330 cm^{-1} which cannot correspond to any atomic disorder (otherwise the Raman signal would be broadband) and which corresponds to a compressive stress up-shifted H6 peak appearing normally at ∼1325 cm^{-1}. This interpretation is in agreement with the so-called Landau No-Go criteria [95–97] explaining why graphenic C–H material cannot exist and which is confirmed with a comparison of stronger chemical bonds and weaker adsorbtion energy of H_2 on graphene [98].

3.6.3. *Gap increase of G-C3N4*

This material is thought to combine high electric conductivity and an appropriate gap (∼1.2/1.8 eV) for water photo-catalysis producing H_2 [99–101] is confronted to undesired gap increase with important electric conductivity decrease because of transformation of G-C_3N_4 into N doped H6 structure with N_2 exodiffusion and N_2 CRER sp3 atomic

rearrangement considering weaker C–N bonds (∼3.16 eV) than C–C (∼7 eV) and N≡N (∼12 eV).

4. Brief Review on up-dated Carbon Raman Spectrometry

4.1. Carbon structures to be considered with Raman spectroscopy

Different types of carbon materials have been identified, including micro and nano-crystalline diamond, amorphous diamond, ta-C, degraded ta-C, ta-C:H, composite diamond-like carbon with the inclusion of sp3 cluster, sp2 cluster and stacks of sp2), a-C:H, a-C (amorphous sp3/sp2 homogeneous mixture), composite graphite-like carbon, glassy carbon (porous mix of fullerenic, DLC and GLC), amorphous graphite, carbon wire and fiber CNW, CNF, single/multiwall CNT, multilayer/single layer graphene, fullerenic and graphenic particles, micro/nano-polycrystalline graphite which have been reviewed in detail elsewhere [41]. Note that most non-crystalline carbon materials *do not fit the general description of "amorphous carbon"* (which by definition does not contain any ordered sp3 and sp2 cluster substructures) [28,29,66,67,102].

Therefore, it is difficult to correctly assign each Raman band and peak when insufficient consideration is brought to peak shift, broadening, and band overlapping. Notwithstanding that very often atomic rearrangement has not been considered, for instance when unexpected D diamond peak appears in a carbon Raman spectrum after annealing of a-C:H which cannot be explained without anomalous atomic rearrangement [29,52] or with some glassy carbon material for instance [31,49,79] when a H6 hexagonal sp3 diamond peak at ∼1325 cm^{-1} is observed different from mislabeled the so-called D-disorder peak at ∼1350 cm^{-1} corresponding to A (armchair) edge graphenic material vibration mode [28].

This is the reason we briefly review the following updated carbon Raman spectrometry fundamentals which must be considered for a detailed description of atomic rearrangement phenomena. These phenomena are reviewed in section III and correspond to several revisited aspects which have been formerly defined [103]. Before looking at carbon Raman spectra assignment, other different characterizing features have to be checked [9]: the sp2/sp3 ratio (for instance with carbon Auger peaks), hardness (density of cohesion energy), stress (recall relation between stress and Raman shift with Pauleau formula [90]), hydrogen content, contamination, thermal stability and elaboration process conditions defining atomic rearrangement (all these depending on precursor material, temperature, impinging particles energy and flux, dissociation, ionization), which have been discussed in more detail in Refs. [9,28].

4.2. Comparison between Raman spectra of different carbon material types

Much of the confusion about Raman peak assignments probably comes from the misfit of quantum mechanics theory and general fundamentals, even though these formulations have contributed to significant scientific progress.

This concerns, for instance, the double resonance Raman scattering theory, the definition of atomic disorder and of the amorphous state, the origin of band broadening, Raman peak up-/downshift (compressive/tensile stress) and especially the so-called mislabeled D-disorder peak at ∼1350 cm^{-1} [28,103–105]. It is all the more confusing that this peak is close to the rhombohedral D diamond peak at ∼1330 cm^{-1} and hexagonal chair structure H6 diamond peak at ∼1325 cm^{-1} [31,80,81,93,94]. It is also confusing because carbon materials grown with different thin film deposition devices can correspond to composite material containing all sorts of substructures [66,67] (summarized in Fig. 1), with properties strongly dependent on their distribution and size.

Confusion also exists on the G-band assignment [62,78,103] originally said to correspond to the Csp2–Csp2 stretching mode, which in fact is the overlapping bands of different more or less stress shifted broader bands corresponding mainly to odd rings C5/C7 (∼1520/1550 cm^{-1}) [108], hexagonal sp2 rings (∼1580 cm^{-1}) corresponding to the stationary phonon mode within such rings [28,109], Csp2–Csp3 (∼1470/1510 cm^{-1}) [61] and edge dangling

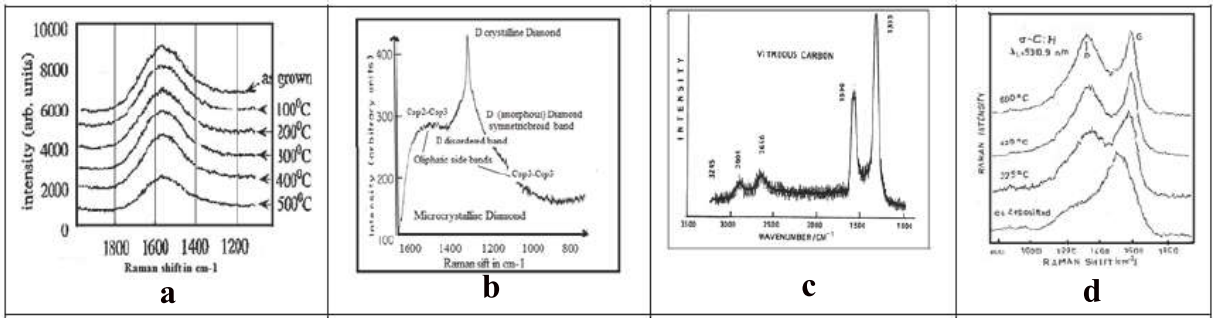

Figure 6. Raman spectra of (a) ta-C (Ta-C by Anders et al. [78] As grown (60 GPa, 80% sp3) $\sim$50 cm^{-1} stress upshift and disorder broadening of Csp2–Csp3, C5/C7 $\sim$1590/1610 cm^{-1}. Csp2–Csp2 $\sim$1640 cm^{-1}. Few sp2 clusters. Annealing 500°C less sp3 (40 GPa, 60% sp3), reduced stress), (b) Nano-diamond (nano-diamond by McNamara et al. [80]. Superimposed Diamond peak on amorphous diamond band ($\sim$1330 cm^{-1}), disordered T band (Csp3–Csp3 $\sim$1100 cm^{-1}) and the so-called D-disorder band ($\sim$1350 cm^{-1}) (GeA-edge phonon being Raman active)), (c) Glassy carbon (Glassy carbon by Huong et al. [31]. Gpeak. 10 cm^{-1} upshifted peak G and D diamond. Weak the so-called D-disorder (GA-edge $\sim$1350 cm^{-1}) coherent with 2D peak $\sim$2700 cm^{-1}. Stress shifted DG $\sim$3000 cm^{-1} Csp3–Csp2–Csp3 overtone of Csp3–Csp2)) and (d) a-C:H (a-C:H annealing by Wagner et al. [52] diamond appears $\sim$1330 cm^{-1}, tensile stress reduced (H_2 exodiffusion) G peak getting sharp (sp2 clusters in sp3 amorphous "diamond-like" matrix).

Csp2–Csp2 ($\sim$1620 cm^{-1}) also IR active [110]. Therefore, the "true" G peak is only to be found for graphenic structure containing sp2 cyclic rings.

Another point of confusion is that the same designation D is currently used for different structures: diamond (crystalline) and disordered (amorphous) diamond [68, 80, 111], D graphene (mislabeled so-called D-disorder peak [103–105,113)],DLC [30,52,62,112] (an amorphous state which is a mix of sp2 and sp3), crystalline defects, isotopes, impurities, interstitials, vacancies, dangling bonds, etc.). Raman spectra of different types of carbon material can show

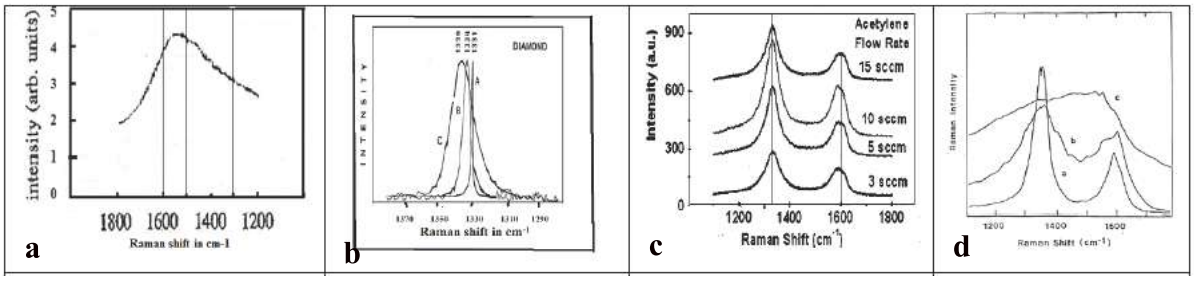

Figure 7. Raman spectra of (a) pseudo-amorphous graphite with few sp3 and amorphous graphite (GAC) (ion irradiated glassy carbon by Prawer et al. [112] $\sim$15 cm^{-1} stress upshift sp3 Diamond band and D-disorder (GeA cluster edge $\sim$1350/1360 cm^{-1}. Max intensity GD band 1560 cm^1 Csp2–Csp3. Weak G-band $\sim$1600 cm^{-1}(sp2 clusters destroyed by irradiation). Similar to non-stressed amorphous graphite 100% sp2 (Rouzaud [102]), (b) crystalline/amorphous diamond (D diamond by Huong et al. [111]. Results showing existence of amorphous diamond (symmetric band $\sim$1330 cm^{-1}. Same frequency than ordered diamond peak. No G peak/band. No sp2 cluster edge GeA band $\sim$1350 cm^{-1} $\Rightarrow$ (no so-called D-disorder at 1350 cm^{-1}). No Csp3–Csp2, no Csp2–Csp3), (c) carbon nanofiber (CNF by Lin et al. [69] G+1580 cm^{-1}, G$^-$ (CNT intern walls 1560 cm^{-1}), main peak for H6 (hexagonal diamond 1325 cm^{-1} (sp2 transformed in sp3 on outer CNT wall during growth process (plasma). No Csp3–Csp2 band (reduced amount only on interface between inner and outer part of CNW)), and (d) modified glassy carbon (Raman spectra glassy carbon N+ irradiated by Iwaki et al. [86] $\sim$40 cm^{-1} stress upshift G$\sim$1610 cm^{-1}, GeA$\sim$1390 cm^{-1}. Amorph. Diamond $\sim$1370 cm^{-1}, sp3–sp2 $\sim$1510 cm^{-1}. Tensile stress downshift ($\sim$30 cm^{-1} with N_2 exodiffusion). Similar to ta-C).

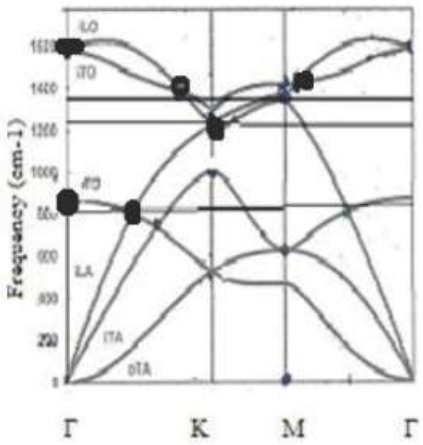

Figure 8. Phonon dispersion curves of graphene by Lazzeri et al. [109]. *G peak at 1580 cm^{-1} corresponds to double degeneracence in-plane phonon mode on Γ point (stationary vibration mode within hexagonal Csp2–Csp2 cyclic ring). *The so-called D-disorder peak at ∼1350 cm^{-1} corresponds to a double degeneracence in-plane phonon mode on near K point (Coupled Double Resonance scattering on a symmetric A-edge Csp2–Csp2 bond (external edge of graphene sheet or intern edge of voids in graphene). *The so-called 2D peak at ∼2700 cm^{-1} corresponds to addition of D-disorder phonon (2K mode on A-edge), and in the bulk to 2 K and 2 M phonon modes Raman active (single M phonon mode at ∼1350 cm^{-1} is not Raman active).

paradoxically quite similar aspects, especially concerning "D" and "G" band, which, however, can be distinguished from their neighbors by looking at band broadening (disorder effect), stress shift and different kinds of atomic rearrangements. The Raman spectra in Fig. 6, corresponding to references [31,52,69,86] can be compared with those in Fig. 7 to some extent and corresponding to [102,112,69,111,86].

It was shown long ago that the D band cannot account for sp3 concentration in carbon material. For DLC material containing some significant amount of sp2 it is shown that the ID/IG ratio (integrated intensity of D and G-band) is proportional to number and size of graphitic crystallites [30]. Those appears during annealing of crystalline diamond above ∼800/900°C [31,61], the size of which depends on annealing temperature and time, because graphite is the thermodynamic carbon ground state. No the so-called "D-disorder" band is observed in large grain polycrystalline graphite and crystalline graphite particles [31,61, meanwhile it is observed for small graphite dust particles [114]. It is therefore necessary to know what the so-called D-disorder peak in reality is, in revisiting Raman spectrometry fundamentals.

4.3. General aspects of Raman fundamentals

4.3.1. *Classical and quantum mechanical description of Raman scattering*

Raman theory based on classical description are reviewed in many published works [115] and has been refined with quantum mechanical aspects involving photon/electron/phonon scattering and with which ordered crystalline structures such as diamond, graphene, CNT could be characterized [28,104,105].

Specific phonon modes diamond [81] and graphene [104] crystalline material can be determined with their wave vector direction, which has been defined with phonon dispersion curves in the reciprocal space. Figure 8 shows the dispersion curves for graphene (by Lazzeri et al. [109]) for many DLC materials where sp2 clusters are nothing other than graphene.

4.3.2. *Role of stress and atomic disorder on Raman shift and band broadening*

In a more complex and disordered structure [116], the number of phonon modes is much higher. However, considering the duality between quantum mechanical representation and classical vibration mechanics, the atomic vibration modes which govern the Raman effect can be qualitatively described with some anharmonic oscillator composed by two atoms of the same mass with interatomic energy potential $U = \alpha x^6$ and force constant $K = 2\alpha x^{-4}$ [117]. Considering that Force constant K is shifted by ΔK by internal stress σ, and phonon frequency is shifted by: $\delta\omega/\omega_0 = \sigma(1-\nu)/E_0$ (Pauleau formula) [90] (ν is the Poisson coefficient, E_0 is the mean elastic constant) this shows that:

*The Raman shift is proportional to internal stress.

In amorphous (disordered) material, the interatomic distance is $x_\mathrm{i} = x_0 + \delta x_\mathrm{i}(\delta x$ distortion) and interatomic energy potential $U = \alpha x^6$ [117] the strain δx_i distribution corresponds also to phonon frequency shift $\delta\omega_\mathrm{i}$ distribution with $\delta\omega_\mathrm{i}/\omega_0 = \eta\delta x/x_0$ [28]. Therefore:

*Band broadening is always associated to atomic disorder.

Frequency well-defined Raman peak ⇒ ordered material structure (constant interatomic bonds).

4.3.3. *Locality of scattering event and confinement effect*

Raman shift anomalies have been generally considered as the consequence of "confinement" of phonon and electrons on edges and smaller particles by modification of their electronic orbital environment [89,103,104,113,118].

However, experimental results are not always in accordance with such calculated and predicted effects. Furthermore, a local phonon vibration mode has been shown with micro Raman on graphene A-edges corresponding to the so-called D-disorder peak ($\sim$1350 cm^{-1}) [119,120]. This can also be deduced from the graphene phonon dispersion curves in the reciprocal space (Fig. 8) [28] for the G Raman peak corresponding to the Γ point at 1580 cm^{-1}, which corresponds to some stationary phonon vibration mode within the hexagonal cyclic sp2 ring. Recall that the wave vector direction in the reciprocal space corresponds to a propagation wave direction in real space. On the Γ point of these curves phonon wave vector direction is perpendicular to the graphene plane for which no phonon wave propagation perpendicular to the plane can exist.

The confinement effect in smaller sp2 clusters based on a Quantum Mechanical calculation appears to be overestimated, when predicted Raman shifts [118] can be also interpreted with other more likely effects [104,28]: as grown a-C:H can be differently stressed (compressive stress or tensile stress) depending on which depositing process has been used (temperature, ion peening, stress relaxation):

(1) Tensile stress can appear during thermal treatment of a-C:H (denser sp3 rearrangement and exodiffusion of H_2) which can then be relaxed [52].
(2) Compressive stress can appear in consequence of growth of sp2 clusters which have lower atomic density (higher volume) than their surrounding amorphous diamond-like material.
(3) Continuing the annealing process, compressive stress will be relaxed. The confinement effect is also overestimated as shown with sp2 cluster optoelectronic gap calculation [89], which is much higher than experimentally measured.

4.3.4. *Double resonance theory and phonon backscattering on edges and defects*

According to the double resonance (DR) theory based on successive Raman scattering events in sp2 clusters and graphene flakes, in addition to the law of energy conservation, the law of impulse conservation has to be fulfilled [113].

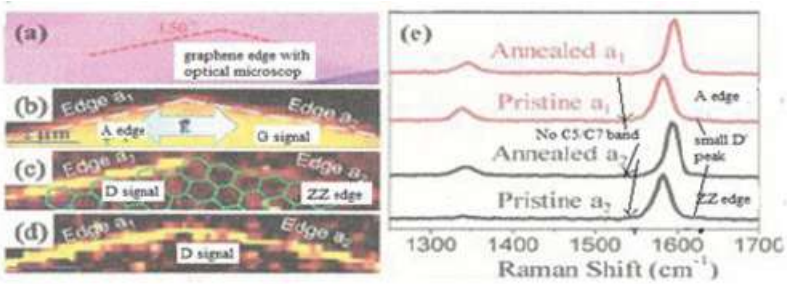

Figure 9. Micro Raman experimental results showing graphene ZZ edge transformation into A-edge with annealing at ∼300°C adapted from Xu et al. [119]. No C5/C7 band at ∼1490/1530 cm^{-1}. Tensile stress downshift ∼15 cm^{-1} on pristine material. The so-called D-disorder peak at 1350 cm^{-1} localized on external A-edge. D indicates spots in the bulk corresponding to internal A-edge of voids. D' peak (corresponding to edge dangling Csp2–Csp2) is reduced with annealing at ∼300°C.

In fact, only the latter is achieved in considering some phonon backscattering on edges and defects [104,28]. Looking at existing phonon modes at ∼1350 cm^{-1} it appears that the so-called D-disorder Raman E ffect can be interpreted in terms of phonon backscattering on ordered A-type (symmetric Armchair) graphene edges, and is therefore mislabeled. This is in agreement with micro-Raman analysis [119,120] (Fig. 9), and also with the point that the corresponding GeA Raman signal is not observed for larger crystallites for which the edge Raman signal is smaller than the background noise of larger bulk material (where that volume/surface ratio is increasing) [28].

The usual quantum mechanic formalism is with delocalized phonons and interprets Double-Resonance backscattering in term of "intra-valley" and "inter-valley" scattering events [103–107] corresponding to adjacent Brilloin zones. However, looking more closely at the energy balance, it appears that this model violates the law of energy conservation. Therefore, a better coherent Couple Double Resonance (CDR) theory model has been developed [28] that obeys the energy conservation law and is based on locality and classical/quantum mechanics dual representation of electron and phonons.

With a short distance between paired electron/hole (Kohn effect) and the important difference of scattering time of the interacting photon, electron and phonon, a CDR backscattered phonon can be either absorbed by an activated electron or by a corresponding valence band hole. This effect is thought to account for Raman Effect coupling and resonance between different phonon modes and overtone modes explaining the dependence of Raman signal with different orientation of polarized laser light, and how the corresponding Raman signal can be local [28].

This model accounts for micro-Raman results of the so-called D-disorder Raman peak and its locality on symmetric A-edge (Armchair shape edge) graphenic materials (including sp2 clusters in DLC). The equivalent CDR Raman peak is not observed on graphene materials such as hexagonal Boron Nitrogen material (hBN) [121] for which A-edge does not correspond to a symmetric oscillator. However, such A-edge can also exist internal to graphenic bulk material in vacancies and voids in agreement with experimental observations on CNT [122,123]. Therefore, such so-called "D-disorder" peak (corresponding to Raman CDR phonon back scattering) can also be observed in the middle of graphene and CNT surface containing vacancies (Fig. 10) corresponding to Raman spectra of Ar irradiated graphene (according to Dresselhaus et al. [105]).

This illustrates a point contrary to the abstract quantum mechanical interpretation with inter valley Raman transition, the sharp D peak at ∼1350 cm^{-1} has in fact nothing to do with disorder but corresponds to CDR of K phonon being backscattered on well-ordered symmetric A-edges. Ar+ ion bombardment of a graphene sheet first creates vacancies and voids (geometric holes in the graphene plane), for which the D and D' peaks stay sharp (ordered edge structure on which dangling Csp2–Csp2 have been formed). Disorder only appears with high Ar ion irradiation with

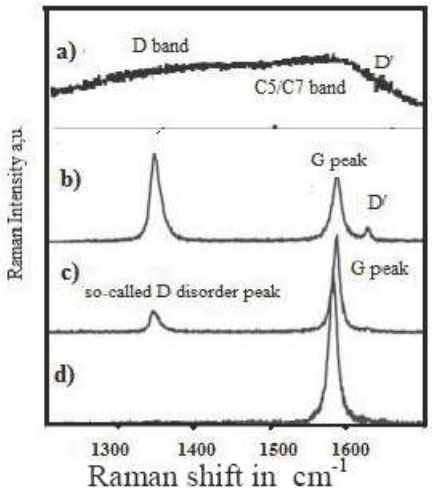

Figure 10. Argon ion irradiated graphene By M.S. Dresselhaus et al. [105]. Disorder band broadening appears only for high ion doses and mislabeled so-called D-disorder peak corresponds in fact to well-ordered GeA-edge. (a) Ion dose >10^{15} producing disordered Graphene. Stress up shifted so-called D-disorder broad band, broad C5/C7 band and broad G-band. No stress shifted broad D' band (disordered edge Csp2–Csp2 dangling bonds). (b) Ion dose 10^{12}. Intense so-called D peak. No peak broadening on D and G peaks. No C5/C7 band. No stress up-shifted D-disorder band and G peak. No stress shifted D' band (edge Csp2–Csp2 dangling bonds). Holes produced by Ar+ impact with intern edge Csp2–Csp2 dangling bonds in ordered graphene material. (c) Ion dose 10^{11}. Sharp $G \sim 10\text{cm}^{-1}$ compressive stress upshift. Few holes (voids) produced by Ar+ impact and few Csp2–Csp2 dangling bonds on void internal edges. For ion dose $< 10^{11}$ no defect formed. Non-stress shifted intense G peak Considering the strong interlinking carbon bonds ($\sim$ 7 eV) higher incident ion energy and higher ion dose are necessary to produce atom removal in defect free graphene.

Table 3. Revised nomenclature for main carbon Raman peaks.

Raman (cm^{-1})	Peak/band	Type of structure	Energy in eV type of structure
$\sim$1330	D-peak	Ordered diamond cubic	Csp3–Csp3
$\sim$1325	DH6 peak	Ordered hexagonal diamond	$\sim$7.02
$\sim$1200/1400	Dd band	Amorphous diamond, ta-C	$\sim$7.015
$\sim$1150	DD	Csp3–Csp3 edge bonds	Aliphatic Csp3–Csp3
$\sim$1470	DG	Csp3– sp2cluster edges	Aliphatic Csp3–Csp2
$\sim$1580	G-peak	Stationary sp2 hexagonal ring	Csp2Csp2 $\sim$7.03 eV
$\sim$1560/1620	G-band	Atomic disorder broadening	Superposed GG, DG GC5/GC7
$\sim$1620	GG	sp2 clusters edge bonds	Csp2–Csp2
$\sim$1470	DG	sp2 on sp3 cluster	Csp2–Csp3
$\sim$1520	GD	sp3 on sp2 cluster	Csp3–Csp2
$\sim$1530	GC5	C5 ring	Fullerene C5 mode 1550 cm^{-1}
$\sim$1550	GC7	C7 ring	(upshift by plane curvature)
$\sim$1350	Ge_A	Graphene A-edges edge	External /internal A-edge 0° CDR
$\sim$1300/1400	Ge_A band	Broadening by edge disorder	$\sim$7.03$\pm$ 0.01 eV
$\sim$2690	G2P	2 phonons GeA graphene CDR	In plane 2K/2M phonon modes
$\sim$150	RBM	CNT	Breathing mode ($\sim$radius)
$\sim$1600	G^+	CNT in plane longitudinal	G Stationary mode
$\sim$1560	G^-	CNT in plane transversal	Curvature Csp2–Csp2

overlapping impact zones and it corresponds to important Raman band broadening.

Considering the confusion about the designation and assignments of Raman peaks and bands which have often appeared in papers published about carbon research, we have proposed some new Raman nomenclature to facilitate carbon material engineering [41] (Table 3).

5. Necessary Conditions for a Bethe Nuclear Reactor Concept

5.1. Temperature-dependent atomic rearrangement activated by H_2 recombination

When the solid state material temperature is sufficient (T >300°C for carbon material) [74], trapped H atoms can diffuse and recombine to form H_2 with high energy release, and can contribute to phase transformation in favor of diamond and a diamond-like structure with quantum electronic activation. This is endothermic and thus, it forms a metastable structure. Meanwhile, when less quantum electronic activation is available, thermal atomic rearrangement in favor of graphite ground state will prevail (exothermic).

Therefore, temperature, material composition and structure dependent atomic rearrangement is to be considered which can be driven upon the structure of desired packing density and electronic distribution [29]. It should be mentioned here that this is also the case for other materials with higher 3D electronic orbitals, for instance, where a more complex electronic orbital distribution have been calculated [42,43,54,63,124] — such as for Cr, Fe, Co, Ni, Cu, Pd, and Ta, having different oxidation states and different s–p–d hybridization states. These can have (roughly described) either hexagonal or cubic structure (including PdH_x, NiH_x, Si, and BN, for instance) and the diffusion and ion penetration depth depend on the structure and relevant orientation [27,47,57,64,65,121,124].

Thermally induced graphitic sp2 degradation of a diamond-like carbon target with heat produced by the p+ ion flux/target discharge can be compensated with quantum electronic activated sp3 rearrangement with H_2 chemical recombination and neutralization energy release (similar to diamond growth in H_2/hydrocarbon gas mixture plasma at temperature >500°C), which can then maintain the original denser disordered/amorphous diamond structure (with some electric conduction properties obtained with B and/or N doping for instance).

Compressive stress with specific local geometric distribution can be produced by different means. These can be exerted particularly on interstitial atoms by their neighboring atoms getting closer to each other with sp3 atomic rearrangement, for instance with ion implantation and ion peening effect (such as He^+, C^+ and CH_x^+) [9,10] when they have sufficient energy (>20 eV for C ions). The latter effect is not observed when the impinging ion has few eV of energy [20,46,68] and are much smaller (p+ having $\times$1000 lower size than atoms).

Heat favors the growth of larger stacks of sp2 clusters and graphite micro crystallites of lower atomic packing density and therefore, can also produce compressive stress [29,52], because graphite has $\sim$1.5 lower packing density than diamond, so this can produce volumetric expansion with such graphitic atomic rearrangement. Therefore, the incorporated H atoms with neutralization of implanted H^+ can be subject to compression with the neighboring atoms up to several 100 MPa, when the diamond is transformed into graphitic material [31,60] (before being thermally relaxed). Considering also ta-C:H produced with some biased plasma depositing [79] for instance and transformation of glassy carbon into harder and denser ta-C with high energy N^+ irradiation [87], H atoms will also be submitted to compressive stress (up to 1000 MPa especially when He^+ is implanted) [76].

However, this compressive stress will only correspond to compressive energy in the 1–10 eV range. That is quite small in comparison to compression energy of about 1–10 keV which is necessary for C/p+ nuclear fusion reaction.

5.2. Chemical properties of substrate material

Dissociation of the H_2 precursor gas has to be achieved either by dissociation with catalytic material (such as boron [9,76] and porous AlNi Raney Nickel [125]), or within arc and plasma discharge [11–13,17,21,22]. However, hydro-

gen can also form low energy chemical bond hydrides [47,63,124] which can be released with heat. From nuclear technology, it is known that materials should be of particular purity (graphite for instance) [126] to avoid any parasite nuclear radiation and absorption and contamination, which might affect the nuclear reaction efficiency.

It should be mentioned here that other non-nuclear chemical reactions releasing energy may be superposed on some nuclear reaction (a hypothesis considered by Fleishman and Pons when they proposed a cold fusion nuclear reaction for the first time [127]).

Nuclear reaction artifacts can be caused by contamination with same products other than those resulting from nuclear reactions. For instance Cu which is always naturally associated to Nickel and difficult to remove with usual Ni metallurgy [128] or Fe residual contamination which can result from high density plasma stainless steel reactor wall erosion like those used for large area depositing and parasite low concentration doping has to be avoided [14–16]. This may be neglected when considering etching (e.g. diamond processing) [17,18].

5.3. Solid state structure

Nuclei having a solid state nuclear fusion potential must have the possibility of being brought in close contact to each other. This is particularly true for low mass material which can more easily diffuse in a solid-state substrate, such as protons and dissociated H atoms [9,47,56]. Dense carbon materials with reduced defects (vacancies) such as graphene, H6 sp3 hexagonal chair diamond, crystalline rhombohedral (cubic) diamond, ta-C (amorphous diamond) and hard glassy carbon (whenever containing pores) have high diffusion barrier properties for H atoms and H_2 molecules [10,41,47,49], in contrast to protons which diffuse even through defect free graphene corresponding to densest diffusion barrier carbon material [51].

Proton diffusion lengths are particularly important for some diamond crystalline orientation offering the so-called "string" channeling capabilities [34–37], much higher than for graphite *c*-axis) [38,46], meanwhile p^+ planar channeling in interplane space between dense hexagonal graphenic planes (MWCNT) is paradoxically much lower because subject to spatial periodic oscillation induced by electron exchange depending on ion energy and initial ion trajectory orientation [39,40,51,129] (this is different from H neutral atoms which can easily diffuse in interplane space between dense sp2 hexagonal graphenic planes) [64,40].

With long range channeling (μm range at room temperature), only a few collisions with carbon nuclei occur. However, channeled H^+ can be scattered by phonon vibration transverse to the H^+ channeling direction similar to what exists with electron channeling and the normal electron conduction mode in conducting solid states. This sort of ion scattering is phonon density (temperature) dependent [130,131] and can strongly reduce the channeling length and enhance the proton electron exchange, which reduces the arriving proton energy [32–38].

In disordered composite and amorphous graphitic carbon structures, where no diffusion channels exist (other's than proton energy losses with electron scattering) the implantation depth is much lower (although having lower atomic packing density) and nevertheless reaches the 1000 nm range for 5 keV H^+ [26]. This explains a priori why dense tetrahedral amorphous carbon (ta-C) is expected to have the highest proton/carbon nucleus collision efficiency. However, in such cases $\sim$80% of impinging proton energy is lost with electron scattering and only $\sim$10% with atomic core scattering [20,32,33], in contrast to hot plasma conditions where colliding particles are mainly composed of the nucleus with no close electronic environment. Therefore, the Lawson criteria [132] that determines optimized conditions of nuclear collisions in hot plasma are not applicable to a nuclear collision in the solid state.

Considering that no nuclear reaction has been observed with p^+/carbon solid state material (we have mentioned in Section 1 and what might have been also consequence of weak proton flux used and reduction of the proton energies with electron and phonon scattering), the first defined conditions may be not be sufficient for the achievement of a Bethe–Weizsäcker fusion reactor. It will be probably necessary to look at the nuclear collision process itself and at any

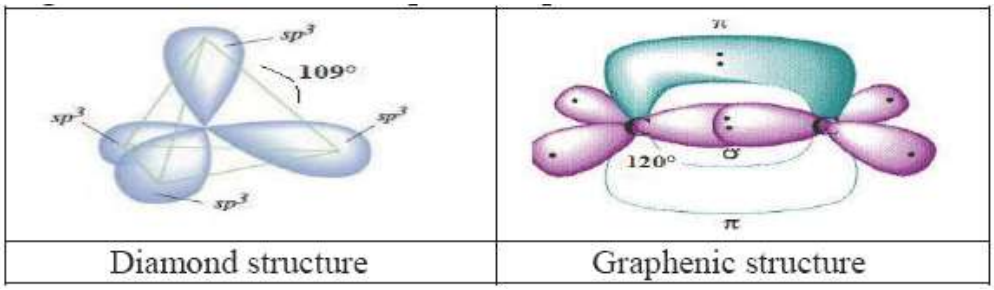

Figure 11. Electron free space for p^+/carbon nucleus collision.

other effects which may facilitate or hamper the nuclear reaction and the overstepping of the nuclear electrostatic barrier.

6. Nuclear Reaction Efficiency

6.1. Electronic orbital screening

It has been shown with laser driven p^+/boron nucleus collisions that the nuclear reaction efficiency is strongly increased when the solid-state boron target surface is transformed into a dense boron plasma, and a significant amount of electrons have left the plasma [7]. However, not all electrons have been stripped off from the boron ionic core. At least 1S electrons are left which apparently has little effect on the p^+/boron nuclear reaction efficiency. It is suggested that a similar situation exists for solid state carbon.

Independent from the reduction of proton energy with electron and phonon scattering (described in Section 3), the anisotropic distribution of sp2 and/or sp3 electronic orbital for which some geometric open space will be left between zones where the electron probability presence is reduced (Fig. 11). Better nuclear reaction efficiency is expected with a dense structure which offers direct access to the atomic nucleus through the electron empty zones.

Amorphous sp3 carbon belonging to a dense atomic structure with large 109° electron open space around the nucleus appears to be the best candidate. Minimum energy reduction of arriving p^+ is provided for a corresponding solid angle. Thus, H_2 chemical recombination energy release activating sp3 atomic rearrangement in ta-C heat degraded (graphitic) is expected to restore the sp3 carbon material structure which favors p^+/carbon nucleus interaction (as long as no crystalline structure is formed and no channeling effect appears).

In addition to these electron depletion zones, some electron stripping of the target solid state carbon material occurs with the photo-electric effect. This is expected to be achievable with a dense luminescent cold plasma working in a pulsed mode, especially when adding some rare gas in the hydrogen plasma in favor of hydrogen gas activation and ionization.

6.2. Proton–carbon nucleus collision cross section

In contrast to longitudinal phonon vibration (stretching modes), transverse phonon C–C vibration (bending modes) which are nearly perpendicular to the arriving fast proton direction can accelerate the proton up to $\sim 2\times 10^5$ eV (proton–electron collision energy when both particles have been accelerated with their electrostatic attraction [133]), before being slowed down in the space between 1S orbital and nucleus (Fig. 12).

This effect is only to be considered with a classical model for which the proton dimension is $\sim$1000 times smaller than the 1S orbital dimension (Bohr radius) [134] and where no negative electric charge exists at the center of 1S

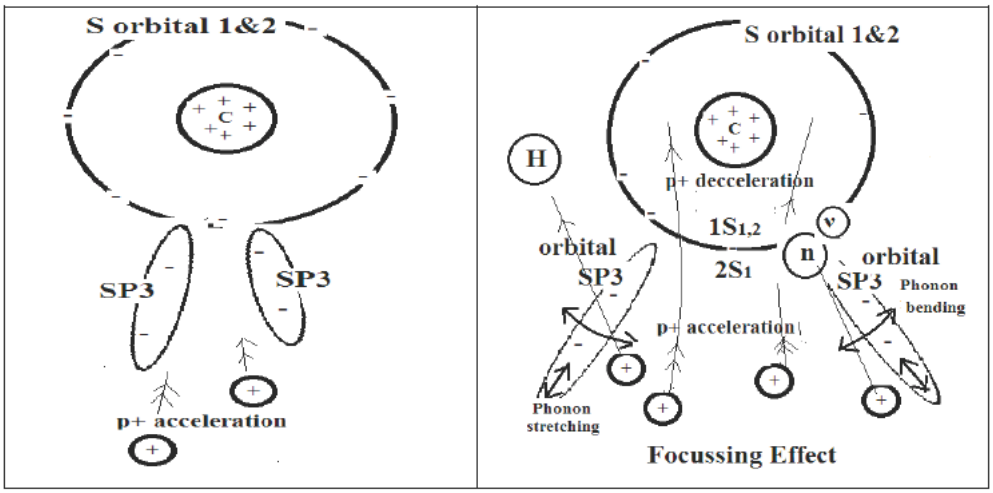

Figure 12. Scheme for p^+ defocussing when sychronic to bending phonon mode.

orbital.

An electrostatic lens defocusing effect of p^+ toward the carbon nucleus is expected, which is stronger than with the quantum mechanical model, because the S electronic orbitals are uniformly distributed over a sphere being superposed to the nucleus zone [42,43]. (It should be noted that the QM description of electron density in the S orbital center does not fit with atomic physical common sense.)

This effect is expected to decrease the p^+/carbon nucleus collision efficiency insofar as the flux of arriving p^+ with a larger solid angle can collide with a lower probability to hit a carbon nucleus (Fig. 12]. Protons will then be slow down and form a hydrogen atom. However, electron capture transforms a proton colliding with an electron in a neutron/neutrino pair which are not affected by the electrostatic barrier [8,135] and which therefore can react with the nucleus in favor of a more deformable electrostatic barrier of a carbon nucleus.

6.3. Anharmonic resonance of electrostatic barrier with phonon/nuclear interaction

Light atoms subject to nuclear fusion (such as He, Li, and Be) have an isotropic spherical electronic environment (1S and 2S electronic shells) which will not significantly modify their nuclear structure, all the more so because strong nuclear binding forces preserve high nucleus rigidity [8,135]. In contrast to heavier elements containing a higher number of charged particles, where the distributed electrostatic repulsion forces weaken the strong force cohesion energy in accordance with the observable Moessbauer effect [42,43], and show nuclear geometric and energy band structure dependence from environmental electronic distribution.

For boron and carbon materials where the 2S/2P electronic orbital can be sp2 and sp3 hybridized with important anisotropic distribution, it is believed that modification of the nuclear electrostatic barrier shape can be more significant than with smaller atoms having only spherical S orbitals. Static anisotropic distribution of the carbon electronic orbitals is expected to be at least able to induce some weak anisotropic deformation of the nuclear electrostatic barrier height [6] (Fig. 13). This will not significantly modify the fusion energy threshold. This is also the case with phonon vibration and electronic oscillation [129,130] which induce nucleus oscillation.

However, in the calculation of the anharmonic resonance effect, it has been predicted that some enhanced tunneling effect occurs during a nuclear collision [136]. Anharmonic resonance between specific phonon vibration modes and a nuclear electrostatic vibration mode may be achievable, considering the multipolar electrostatic configuration of a carbon nucleus and the non-linear electrostatic interaction between electrons and nucleus. With such resonant phonon/nuclear coupling it is then expected there will be a higher vibration amplitude of the nuclear electrostatic barrier.

Similar to the synchronic gating effect of phonon/conduction electron transport mechanism with which superconductivity can be described [130], a proton can more easily move through the oscillating electrostatic barrier when its displacement is synchronic to some specific phonon vibration, corresponding to a tunneling effect enhancement. This is what is to be qualitatively expected with ta-C carbon sp3 longitudinal and transversal phonon vibration frequency (1100/1400 cm^{-1} range) and arriving p^+ velocity (1 keV energy range) corresponding to displacement velocity $\sim 10^5$ m/s and interatomic bypassing frequency $\sim 10^{15}$. These phonon vibration frequencies phonon can be activated with VIS/UV radiation ($\sim$5 eV). Meanwhile at this stage no quantitative detailed results can be obtained with usual abstract quantum mechanical formalism.

Therefore, it is suggested that we look at some improved wave physical description of involved particles with can give clearer insight into the nuclear electrostatic barrier tunneling mechanism with which p^+ can more easily step across the electrostatic nuclear barrier.

7. Perspectives on Improved Physical Description of Quantum Mechanical Effects

Many results predicted with the abstract Quantum Mechanical formalism have been in agreement with experimentally observed effects. However, questions appear when more complex systems are considered, especially questions about the physical nature of the particle/wave duality [137]. Several unanswered questions remain, for instance, the origin of the limited absolute light velocity and significance of mass/energy equivalence, electric charge and different fields beyond the observed effects for which different concepts have been defined [138]. Examples can be given with the failing physical description of single particle interference effects [139]; physical description and material specificity predictions about superconductivity [140]; Raman double resonance theory where the so-called mislabeled D-disorder Raman peak is interpreted [103–105]; intrication phenomena and anomalous compressibility of condensed matter [141]; and the tunneling effect for colliding particles when no barrier width is considered [8]. Other questions arise

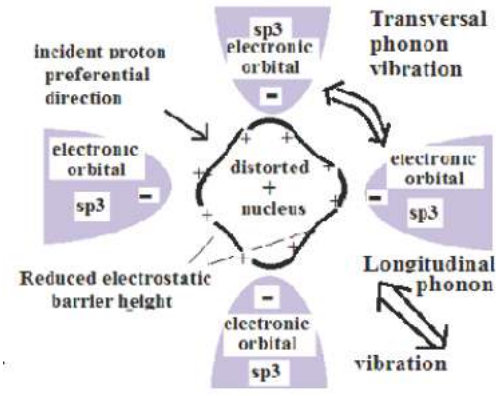

Figure 13. Scheme of electrostatic nuclear barrier distortion with 109° open space sp3 orbital.

about the predicted existence and properties of cubic C3N4, which is supposed to have higher hardness than diamond [86,142] and about the existence of the so-called graphane material [93–98].

Roughly summarized, here is what we propose to be developed in more detail elsewhere. We suggest the main cause of many QM failures is linked to the arbitrary association of an abstract wave function which for many more complex subjects do not correspond to any usual physical wave [137,143], and that the time-dependent evolution of particles described with the Schrödinger equation is based on an approximate dual wave/particle physical description, which can sometimes lead to absurd conclusions, for instance the Schrödinger cat paradox, in which the cat is alive and dead at the same time; or more prosaically when the so-called D and D' disorder peaks in graphene are interpreted as abstract quantum mechanical effects, in contradiction with elementary observable solid state physical effects [28,105]. Several aspects of quantum mechanical fundamentals have also been questioned with more general theoretical consideration [144]).

It is then suggested that instead of a vacuum, some elastic non-viscous aether exists, which has variable density of cohesion energy (potential energy) and where local perturbation can generate waves with light propagation velocity according to formulae $c = \sqrt{(k/\varrho_0)}$ and considering density of cohesion energy is equivalent to mass density and considering that density of thermal energy (nkT/volume) is defining the pressure of an ideal gases. It is known how wave packets formed with waves of different phase can have group velocity V_g, and considering their mean wave energy density amplitude *A*, some intrinsic wave packet energy can be defined with $E_\mathrm{pk} = \frac{1}{2}kA^2 = mc^2$ defining mass *m* and kinetic energy $E_\mathrm{c} = \frac{1}{2}mV_\mathrm{g}^2$. Particle size is defined with the volume occupied by wave-packet wave length and energy wave amplitude in a 3D vortex (Eddy). 3D fluid dynamics [145] and wave oscillating modes with longitudinal and transversal modes for which complex mathematical treatment will have to be developed, similar to what has been developed with atmospheric phenomena and 3D wave modelling in liquids [146,147]. With such a model, nuclear particles could no longer be considered in terms of association of sub-particles sticking together with mysterious weak and strong cohesion forces, but resulting from a split of original larger particle wave packets having its own size, mass and electric charge. This model is then expected to provide some physical description of nuclear tunneling effects, enabling us to sort out optimized solid state nuclear reaction conditions.

8. Conclusions

With this analysis, we have shown some of the expected feasibility of a solid state Bethe CNO cycle solid state nuclear fusion reactor for the specific structure of amorphous tetrahedral carbon (ta-C), which is:

(1) A particularly dense material which can be regenerated with the proton flux.
(2) In an amorphous state with which atomic core scattering along μ m proton implantation depth range (for 1 keV range proton energy) can be kept significant in comparison to electronic exchange which reduces the arriving proton energy.

The theoretical ratio of produced/consumed energy appears to be in the range of 10–100 when no electronic screening remains during the nuclear collision process, comparing the conditions of proton/carbon nucleus reaction with similar proton/boron reaction results. Uncertainty remains about transposing proton/boron results to proton/carbon reaction with a lower nuclear reaction energy threshold. This uncertainty is expected to be cleared up with similar experiment with a laser driven proton/boron reaction. The collision and fusion efficiency is expected to be improved with phonon/proton interaction and phonon/nucleus anharmonic resonance with which a proton flux – being synchronic to coupled phonon/nuclear electrostatic vibration – can more easily get through the nuclear electrostatic barrier. At this stage, it appears the limitation of conventional quantum mechanical formalism which fail to produce better physical insight into the wave structure of subatomic particles, and with which different wave interference mechanisms and the nuclear electrostatic barrier tunneling effect might be clearly sorted out.

Considering that abstract quantum mechanical formalism has also failed in many other ways, we suggest revisiting fundamentals with a new separate investigation on some aether model with which 3D fluid and wave mechanics can give account of all acquired data with a dual wave/particle description QM particle/wave duality. This should also give clearer insight into the interference mechanisms and nuclear electrostatic barrier tunneling effect. Meanwhile experimental investigation into this phenomenon will have to be organized.

References

[1] G. Mondet, Thesis. Propriétés radiatives des plasmas de fusion. Emissivité et opacité dans des structures atomiques complexes, Université Paris Sud - Paris XI, France, 2013.

[2] M.R. Gomez, S.A. Slutz, A.B. Sefkow, D.B. Sinars, K.D. Hahn, S.B. Hansen, E.C. Harding, P.F. Knapp, P.F. Schmit, C.A. Jennings, T.J. Awe, M. Geissel, D.C. Rovang, G.A. Chandler, G.W. Cooper, M.E. Cuneo, A.J. Harvey-Thompson, M.C. Hermann, M.H. Hess, O. Johns, D.C. Lampa, M.R. Martin, R.D. McBride, K.J. Peterson, J. L. Porter, G. K. Robertson, G. A. Rochau, C. L. Ruiz, M. E. Savage, I. ?C. Smith, W. A. Stygar and R. A. Vesey, Experimental demonstration of fusion-relevant conditions in magnetized liner inertial fusion, *Phys. Rev. Lett*. **113** (2014) 155003.

[3] H.L. van der Horst, VIIIc Neutron Generators, gas-discharge tubes, Philips Technical Library**16**. Eindhoven, Netherlands, Philips Technical Library (1964) 281–295.

[4] J. Reijonen, Compact neutron generators for medical, homeland security, and planetary exploration, *Proc. 2005 Particle Accelerator Conference,* Knoxville, Tennessee, pp. 49–53.

[5] J.M. Elizondo-Decanini, D. Schmale, M. Cich, M. Martinez, K. Youngman, M. Senkow, S. Kiff, J. Steele, R. Goeke, B. Wroblewski, J. Desko and A.J. Dragt, Novel surface-mounted neutron generator, *IEEE Trans. Plasma Sci*. **40** (9) (2012) 2145–2150.

[6] J. Huizenga, N. Ramsey, A.J. Bard, N. Hackerman, S.E. Koonin, J. Bigeleisen, J. Landis, H.K. Birnbaum, P. Lipman, M. Boudart, B. Miller, C.F. Callis, D. Nelson, M. Desselhaus, J. Schiffer, L. Faulkner, J. Schoettler, T. K. Fowler, D. Stein, R.L. Garwin, M. Wrighton and J. Gavin, Cold Fusion research, A Report of the Energy Research Advisory Board to the United States Department of Energy (1989) DOE/S-0073 DE90 005611.

[7] C. Labaune, C. Baccou, S. Depierreux, C. Goyon, G. Loisel, V. Yahia1 and J. Rafelski, Fusion reactions initiated by laser-accelerated particle beams in a laser-produced plasma, *Nature Commun*. 4 (2506) (2013).

[8] K.S. Krane, *Introductory Nuclear Physics (Bethe cycle)*, Wiley, New York, 1988, p. 537.

[9] S. Neuville and A. Matthews, *Thin Solid Films* **515** (2007) 6619.

[10] R. McKenzie, D. Muller, B.A. Pailthorpe, Z.H. Wang, E. Kratchinskaia, D. Segal, P.B. Lukins, P.D. Swift, P.J. Martin, G. Amaratunga, P.H. Gaskel and A. Saeed, *Diamond and Related Materials* **1**(1) (1991) 51.

[11] B.K. Tay, X. Shi, L.K. Cheah and D.I. Flynn, *Thin Solid Films* **308,309** (1997)199.

[12] A. Hurkman, D.B. Lewis and W.-D. Münz, *Surf. Eng.* **19** (Part3) (2003) 205.

[13] C. Corbella, I. Bialuch, M. Kleinschmidt and K. Bewilogua, Modified DLC coatings prepared in a large-scale reactor by dual microwave/pulsed-DC plasma-activated chemical vapour deposition, *Thin Solid Films* **517**(3) (2008)1125–1130.

[14] M. Liehr, F. Fendrych, A. Taylor and M. Nesládek, Routes towards large area, low pressure nanodiamond growth via pulsed microwave linear antenna plasma chemistry, *MRS Proceedings*, Vol. 1282 (2011). DOI: https://doi. org/10. 1557/opl. 2011. 524.

[15] A. Kromka, O. Babchenko, T. Izak, K. Hruska and B. Rezek, Linear antenna microwave plasma CVD deposition of diamond films over large areas, *Vacuum* **86** (2012)776–779.

[16] H.A. Mehedia, J. Acharda, D. Rats, O. Brinza, A. Tallairea, V. Millea, F. Silva, C. Provent and A. Gicquel, *Diamond and Related Materials* **47** (2014) 58–65.

[17] S.J. Pearton, A. Katz, F. Ren and J.R. Lothian, ECR plasma etching of diamond, Electronics Lett. **28** (1992) 822.

[18] D. T. Tran, T.A. Grotjohn, D.K. Reinhard and J. Asmussen, Microwave plasma-assisted etching of diamond, *Diamond and Related Materials* **17** (4–5) (2008)717–718.

[19] R.A. Dandl, J.L. Dunlap, H.O. Eason, P.H. Edmonds, A.C. England, W.J. Herrmann and N.H. Lazar, Electron cyclotron heated "target" plasma experiments, Plasma Physics and Controlled Nuclear Fusion Research, *Proc. Third Int. Conf. Plasma*

Physics and Controlled Nuclear Fusion Research, Novosibirsk, USSR (Russian Federation), 1–7 Aug. 1968. International Atomic Energy Agency, Vienna (Austria), Vol. II, No. 3, 1969, pp. 435–447, IAEA-CN–24/J-6; ISSN 0074-1884.

[20] Andre Anders (Ed.), *Handbook of Plasma Immersion Ion Implantation and deposition,* Wiley, New York, 2000, ISBN 0-471-24698-0.

[21] A.A. Galeev and R.N. Sudan (Eds.), *Basic Plasma Physics I. Volume I of Handbook of Plasma Physics*, North-Holland, Amsterdam, New York, 1985.

[22] J.A. Bittencourt, *Fundamentals of Plasma Physics*, Springer, Berlin, 2004. ISBN 9780387209753.

[23] S.M. Pfotenhauer, O. Jäckel, A. Sachtleben, J. Polz, W. Ziegler, H.P. Schlenvoigt, K.U. Amthor, M.C. Kaluza, K.W.D. Ledingham and R. Sauerbrey, *New J. Phys.* **10** (2008) 033034 (14pp.).

[24] J. Winter, *J. Nucl. Mater.* 131(1987)145–147.

[25] J.P. Coad, A.S. Kaye, C. Walker, A.J. Avery, D.J. Diskett and R.E. Walker, EMRS Meeting XVII, Proceedings by P. Koidl and P. Oelhafen, Les Editions de la Physique (Eds.) (1987) 417.

[26] J. Eck and M. Balat-Pichelin, *Vacuum* **85**(3, 24) (2010) 380–389.

[27] M. Balat-Pichelin, J. Eck, S. Heurtault and H. Glénat, *Appl. Surface Sci.* **314** (2014) 415–425.

[28] S. Neuville, Carbon Structure Analysis with Differentiated Raman Spectroscopy (Lambert Academic Publishing Eds.), 2014, ISBN978-3-659-48909-9.

[29] S. Neuville, *Surf. Coat. Technol.***206** (4) (2011) 703.

[30] F. Tuinstra and J.L. Koenig, *J. Phys. Chem.* **53** (1979) 1126.

[31] P.V. Huong, *Diamond Related Mater*. **1** (1991) 33.

[32] B. Gervais, M. Beuve, G.H. Olivera and M.E. Galassi, Numerical simulation of multiple ionization and high LET effects in liquid water radiolysis, *Radiation Phys. Chem.* 7**5** (2006) 493–513.

[33] S.O. Kucheyev, *Ion Beam Processing*, Handbook of Material Pocessing, Chapter III, R. Groza (Ed.), Taylor and Francis Group CRC Press, Boca Raton, Florida, 2007.

[34] T.E. Derry, Thesis /Dissertation Ion channelling in diamond. University of the Witwatersrand, Johannesburg (South Africa), 1978, Iaea. Org/inis/collection/NCLCollectionStore/Public/10/446/10446597.

[35] B. Schmiedeskamp, P. Jonk, H.E. Roosendaal and H.O. Lutz, *J. Nucl. Instr. Methods Phys. Res. Section B* **17** (4) (1986) 309–313.

[36] M. Moneta and J. Czerbniak, Influence of electron exchange on planar channeling of protons in diamond, *Nucl. Instr. Methods Phys. Res. Section B* **48**(1) (1990) 142–144.

[37] A.V. Bagulya, O.D. Dalkarov, M.A. Negodaev, A.S. Rusetskii, A.P. Chubenko, V.G. Ralchenko and A.P. Bolshakov, Channeling effect in polycrystalline deuterium-saturated CVD diamond target bombarded by deuterium ion beam, Phys. Ins.Det. (2014) 1-8. ArXiv: 1408. 7109. DOI: 10.1016/j.nimb.2015.01.021. On-line Cornell University Library. Ithaca, NY.

[38] D. Schroyen, M. Bruggeman, I. Dezsi and G. Langouche, Ion Implantation in highly oriented pyrolytic Graphite, *Nucl. Instr. Methods Phys. Res. Section B* **15** (1986) 341–343.

[39] A.V. Krasheninnikov and K. Nordlund, Channeling of heavy ions through multi-walled carbon nanotubes, *Nucl. Instr. Methods Phys. Res. Section B* **228** (2005) 21–25.

[40] D. Borka, S. Petrovíc and N. Něskovi, Channeling of protons through carbon nanotubes (2011). ArXiv: 1111. 1905v1 (Cond-Mat.Mes-Hall) (2011)1–58. On-line Cornell University Library. Ithaca, NY.

[41] S. Neuville, New Application Perspective for Tetrahedral Amorphous Carbon Coatings QScience Connect 2014:8 http://dx. doi. org/10. 5339/connect. 2014. 8.

[42] L. Eyges, Physics of the Moessbauer effect, *Am. J. Phys*. **33** (10) (1965) 790–802.

[43] V. Schuenemann and H. Paulsen, *Moessbauer Spectroscopy*, Wiley, New York, 2007. ISBN 978-0-470-03217-6.

[44] R.W. Cahn and P. Haasen (Eds.), *Physical Metallurgy*, Fourth Edition, Elsevier, Amsterdam, 1996. ISBN: 978-0-444-89875-3.

[45] T.J. Carter and L.A. Cornish, *Eng. Failure Analysis* **8**(2) (2001) 113–121.

[46] M.S. Dresselhaus and R. Kalish, *Ion Implantation in Diamond, Graphite and Related Materials*, Springer, Berlin, 1992.

[47] L. Schlapbach and A. Züttel, Review article hydrogen-storage materials for mobile applications, *Nature* **414** (2001)353–358.

[48] D.F. Shriver, P.W. Atkins and C.H. Langford, *Inorganic Chemistry,* Oxford University Press, New York, 1989, p. 337.

[49] O.J. A. Schueller, S.T. Brittain, C. Marzollin and G.M. Whitesiders, Fabrication and characterization of glassy carbon

MEMS, *Chem. Mater.* **9**(6) (1997) 1399âĂŞ1406 DOI: 10.1021/cm960639v
[50] Y. Lin, L. Zhang, H.K. Mao, P. Chow, Y. Xiao, M. Baldini, J. Shu and W. Mao, *Phy. Rev. Lett.* **107** (2011) 175504.
[51] Q. Zhang, M. Ju, L. Chen and X.C. Zeng, Differential permeability of proton isotopes through graphene and graphene analogue monolayer, *J. Phys. Chem. Lett*. **7** (17) (2016) 3395–3400.
[52] J. Wagner, M. Ramsteiner, C. Wild and P. Koidl, EMRS XVII, Proceedings by P. Koidl and P. Oelhafen, Les Editions de la Physique. Paris (France), 1987, p. 351.
[53] Y. Wang, D. Connétable and D. Tanguy, *Phys. Rev.* B **91** (2015) 094106 44.
[54] P. Jakupi, J.J. Noel and D.W. Shoesmith, *Electrochemical and Solid States Lett.* **13**(3) (2010) C1–C3.
[55] M.A. Stopher, P.E.J. Rivera-Diaz-del-Castillo, *Mat. Sci. Technol.* **32** (11) (2016) 1184–1193.
[56] V. Demetriou, Study of the Effect of Hydrogen charging on the tensile properties and microstructure of four variant heat treatments of alloy 718, *Int. Conf. Adv. Energy Materials*, AEM-2016, Guildford, UK, ID 54.
[57] A. Ohl and J. Röpke, *Diamond and Related Materials* **1** (1992) 243.
[58] P. Roca I Cabarrocas and N. Layadi, *J. Vac. Sci. Technol. A* **16** (2) (1998)436.
[59] P.W. May, M. Clegg, T.A. Silva, H. Zanin, O. Fatibello-Filho, V. Celorrio, D.J. Fermin, C.C. Welch, G. Hazell, L. Fisher, A. Nobbse and B. Sue, Doped diamond-coated 'black silicon' as a promising material for high-surface-area electrochemical electrodes and antibacterial surfaces, *J. Mater. Chem. B* **4** (2016) 5737–5746.
[60] X. Liu, P. Coxon, M. Peters, B. Hoex, J. Cole, D. Fray, Black silicon: fabrication methods, properties and solar energy applications, *Energy Environ. Sci.* **7** (10) (2014) 3223–3263.
[61] L. Fayette, B. Marcus, M. Mermoux, G. Tourillon, K. Laffon, P. Parent and F. Le Normand, *Phys. Rev. B* **57** (22) (1998) 1412.
[62] J. Robertson, *Diamond and Related Materials* **3** (1994) 732.
[63] N.W. Ashcroft and N.D. Mermin, *Solid State Physics*, Cornell University, College Publishers Harcourt, New York, 1976, ISBN 978-0-03-083993-1.
[64] A. Houari, S.F. Matar and V. Eyert, *Phys. Rev. B* **82** (2010) 241201.
[65] B. Aufray, A. Kara, S. Vizzini, H. Oughaddou, C. Léandri, B. Ealet and G. Le Lay, *Appl. Phys. Lett.* **96** (18) (2010) 183102.
[66] J.L. Bredas and G.B. Street, EMRS Meeting XVII, Proceedings by P. Koidl and P. Oelhafen, Les Editions de la Physique (Eds.), 1987, p. 237.,
[67] D.G. Liu, J.P. Tu, C.F. Hong, C.D. Gu and S.X. Mao, *Surf. Coat. Technol.* **205** (2010) 152.
[68] P.K. Bachmann and W. vanEckervort, *Diamond and Related Materials* **1** (1992)1021.
[69] Y.Y. Lin, H.W. Wei, K.C. Leou, H. Lin, C.H. Tung, M.T. Wei, C. Lin, C.H. Tsai, *JVST* B **24**(1) (2006) 97.
[70] M. Endo, Grow Carbon fibers in the vapor phase, *Chemtech* (September1988) 568576.
[71] J. Campos-Delgado, Y.A. Kim, T. Hayashi, A. MorelosGomez, M. Hofmann, M. Endo, H. Muramatsu, H. Terrones, R.D. Shull, M.S. Dresselhaus and M. Terrones, *Chem. Phys. Lett.* **469** (2009) 177182.
[72] G. Flamant, R. Guillard and D. Laplaz, *Le Vide* **2,4** (300) (2001) 266.
[73] S. Weissmantel, G. Reisse and D. Rost, *Surf. Coat. Technol.* **188–189** (2004) 268.
[74] A. Grill, *Surf. Coat. Technol.* **94,95** (1997) 507–513. .
[75] F. Sato, N. Saito, Y. Hirano, A.H. Jayatissa, K. Takizawa, S. Kavado, T. Kato, H. Sigiyama and M. Ando, *J. Vac. Sci. Technol.* **16** (4) (1998) 2553.
[76] S. Neuville, A. Taggliaferro, Y. Bounouh, S. Vallon, R. Etemadi, J. Perrin, CIP 95 Antibes, Le Vide, Sciences, Techniques et Applications, 64 by SFV (Eds), Paris (France), Vol. 275 (1995).
[77] S. Neuville, *Diamond and Related Materials* **11** (2002)1721–1730.
[78] S. Anders, J.W. Ager III, G.M. Pharr, T.Y. Tsui and I.G. Brown, *Thin Solid Films* **308,309** (1997) 186.
[79] A.P. Badzian, P.K. Bachmann, T. Hartnett, T. Badzian and R. Messier, EMR Meeting XVII, Proceedings by P. Koidl and P. Oelhafen, Les Editions de la Physique Paris (France) (1987) 63.
[80] K.M. McNamara, K.K. Gleason, G.J. Vestyck and J.E. Butler, *Diamond and Related Materials* **1** (1992) 1145.
[81] K.E. Spear, A.W. Phelps, W.B. White, *J. Mater. Res.* **5** (1990) 2277.
[82] D. Rai, H. Joshi, A.D. Kulkarni, S.P. Gejji and R.K. Pathak, Electric field efects on aromatic and aliphatic hydrocarbons, *J. Phys. Chem. A.* **111**(37) (2007) 9111–9121.
[83] K.S. Sankara-Reddy and M. Satyam, Structural ordering of diamond-like carbon films by applied electric field, *Solid State*

Commun. **93** (10) (1995) 797799.
[84] S. Neuville, *Sensors and Actuators* B **121** (2) (2007) 436.
[85] C.E. Borroni-Bird and D.A. King, *Rev. Sci. Instrum.* **62** (9) (1991) 2177.
[86] S. Neuville and A. Matthews, *MRS Bulletin* **22** (9) (1997) 22–26.
[87] M. Iwaki, K. Takahashi and A. Sekiguchi, *J. Mat. Res.* **5** (1990) 2562.
[88] D. Beeman, J. Silvermann, R. Lynds and M.R. Anderson, *Phys. Rev. B* **30** (1984) 870.
[89] J. Robertson and E.P. O'Really, *Phys. Rev. B* **35** (1987) 2946.
[90] Y. Pauleau, in C. Donnet and A. Erdemir, *Tribology of DLC*, Springer, New York, 2008, 102.
[91] A. Erdemir, M. Switala, R. Wei and P. Wilbur, *SurFace and Coatings Technology* **50** (1991)17.
[92] X.H. Wang, G.H.M. Ma, W. Zhu, J.T. Glass, L. Bergman, K.F. Turner, R.J. Nemanich, *Diamond Relat. Mater.* **1** (1992) 828.
[93] J.O. Sofo, A.S. Chaudhari and G.D. Barber, *Phys. Rev. B* **75, 153401** (2007). "Graphane: A two-dimensional hydrocarbon". Physical Review B 75 (15) (2007) 153401–153404.
[94] D.C. Elias, R.R. Nair, T.M.G. Mohiuddin, S.V. Morozov, P. Blake, M.P. Halsall, A.C. Ferrari, D.W. Boukhvalov, M.I. Katsnelson, A.K. Geim and K.S. Novoselov, *Science* **323** (5914) (2009). Evidence for Graphane.
[95] J.C. Tolédano and P. Tolédano, *The Landau Theory of Phase Transitions*, World Scientific, Singapore, 1987, ISBN 9971500256.
[96] P. Tolédano and V. Dmitriev, *Reconstructive Phase Transitions in Crystals and Quasicrystals*, World Scientific, Singapore, 1996, ISBN 9810223641.
[97] T.S. Jackson, G. Möller and R. Roy, Geometric stability of topological lattice phases, *Nature Communications* **6**(Article number: 8629) (2015). doi:10. 1038/ncomms9629.
[98] G.K. Sunnardianto, Storing-hydrogen process on graphene activated by atomic-vacancy, *Int. Conf.on Adv. Energy Materials AEM-2016*, Guildford, UK, ID 54.
[99] N. Martsinovich, Computational design of carbon nitride photocatalysts for water splitting, *Int. Conf. on Avanced Energy Materials AEM-2016*, Guildford, UK. ID 132.
[100] N.B. Makarova, Catalytic naphthalene condensation as a means of producing nanostructured graphene: computational studies, *Int. Conf. on Advanced Energy Material Guildford AEM-2016*, Guildford, UK. ID133.
[101] P. Klán and J. Wirz, *Photochemistry of Organic Compounds: From Concepts to Practice*, Wiley, Chichester, 2009, ISBN 978-1405190886.
[102] J. Rouzaud, A. Oberlin and C. BenyBassez, *Thin Solid Films* **105**(1) (1983) 75–86.
[103] A.C. Ferrari, *Diamond and Related Materials* **11**(3–6) (2002)1053–1061.
[104] L.M. Malard, M.A. Pimenta, G. Dresselhaus and M.S. Dresselhaus, Raman spectroscopy in graphene, *Phys. Reports* **473**(5–6 (2009)51–87.
[105] M.S. Dresselhaus, A. Jorio, A.G. SouzaFilho and R. Saito, *Phil. Trans. Roy. Soc. A* **368** (2010) 5355–5377.
[106] L.G. Cançado, M.A. Pimenta, B.R. Neves, M.S. Dantas and A. Jorio, *Phys. Rev. Lett.* **93** (2004) 247401.
[107] L.G. Cançado, M.A. Pimenta, B.R. Neves, G. MedeirosRibeiro, T. Enoki, Y. Kobayashi, K. Takai, M.S. Dantas, K. Fukui, M.S. Dresselhaus, R. Saito and A. Jorio, *Phys. Rev. Lett.* **93** (2004) 047403.
[108] B. Marcus, L. Fayette, M. Mermoux, L. Abello and G. Lucazeau, *J. Appl. Phys.* **l4** (1994) 3463.
[109] M. Lazzeri, C. Attaccalite, L. Wirtz and F. Mauri, *Phys. Rev. B* **7** (2008) 081406.
[110] B. Dischler, EMRS Meeting XVII, Proceedings by P. Koidl and P. Oelhafen, Les Editions de la Physique (Eds) Paris (France) (1987) 189.
[111] P.V. Huong, B. Marcus, M. Mermoux, D.K. Veirs and G. Rozenblatt, *Diamond and Related Materials* **I** (1992) 869.
[112] S. Prawer, F. Ninio and I. Blanchonette, *J. Appl. Phys.* **68** (1990) 2361.
[113] T.E. J. Dallas, Thesis Structural Phases of Disordered Carbon Materials, Texas Tech University, 1996.
[114] R. Rammamurti, V. Shanov, R. Singh, S. Mamedov and P. Boolchand, *J. Vac. Sci. Technol. A* **24**(2(2006) 179.
[115] R. Singh, C.V. Raman and the discovery of the Raman Effect, *Phys. in Perspective* (PIP) **4** (4) (2002) 39420.
[116] R. Zallen, *The Physics of Amorphous Solids*, Wiley, New York, 1983.
[117] J. Maultzsch, S. Reich and C. Thomsen, *Phys. Rev. B* **70** (2004) 155403.
[118] R. Saito, A. Jorio, A.G. Souza Filho, G. Dresselhaus, M.S. Dresselhaus and M. A. Pimenta, *Phys. Rev. Lett.* **88** (2002) 027401.

[119] Y.N. Xu, D. Zhan, L. Liu, H. Suo, Z.H. Ni, T.T. Nguyen, C. Zhao and Z. X. Shen, *ACS Nano* **5** (1) (2011) 142.
[120] Y.M. You, Z.H. Ni, T. Yu and Z.X. Shen, *Appl. Phys. Lett.* **93** (2008) 163112.
[121] B. Fakrach, A. Rahmani, H. Chadli, K. Sbai and J.L. Sauvajol, *Physica E* **41**(2009) 1800.
[122] K.A. Ritter and J.W. Lyding, The influence of edge structure on the electronic properties of graphene quantum dots and nanoribbons, *Nat. Mater.* **8** (2009) 235–242.
[123] U. Ritter, P. Scharff, C. Siegmung, O.P. Dimmytrenko, N.P. Kulisch, Y.I. Priylutskyy, N.M. Belyi, V.A. Gubanov, S.V. Lizunova, V.G. Poroshin, V.V. Shlapatskaya and H. Bernas, *Carbon* **44**(2006) 2694.
[124] A.J. Smith and D.L. Trimm, *The Preparation of Skeletal Catalysts*, *Ann. Rev. Mat. Res.* **35** (2005)127–142.
[125] W.M. Mueller, J.P. Plackedge and G.G. Libowitz, *Transition Hydrides*, Academic Press, New York, London, 1968.
[126] L.M. Currie, V.C. Hamister, H.G. Mac Pherson, The Production and Properties of Graphite for Reactors, National Carbon Company, 1955.
[127] M. Fleischmann, S. Pons, M.W. Anderson, L.J. Li and M. Hawkins, Calorimetry of the palladium–deuterium-heavy water system, *J. Electroanal. Chem.* **287** (1990) 293–348.
[128] F. Crundwell, M. Moats, V. Ramachandran, T. Robinson and W.G. Davenport, *Extractive Metallurgy of Nickel, Cobalt and Platinum Group Metals*, Elsevier, Amsterdam, 2011. ISBN: 978-0-08-096809-4.
[129] V.V. Cheianov and V.I. Fal'ko, Friedel oscillations, impurity scattering, and temperature dependence of resistivity in graphene, *Phy. Rev. Lett*. **97** (22) (2006) 226801–226804.
[130] S. Neuville, Superconductivity described with electron–phonon synchronic coupling, *1st Int. Conf. on Advanced Energy Materials*, 2016, ANM-3, Guildford, UK, to be published in Materials to Day.
[131] R.J. Kamaladasa and Y.N. Picard, Science, Technology, and Application. A. Méndez-Vilas and J. Díaz (Eds.), 2010, Formatex Research center C/ ZurbarÃąn 1, 2Âž - Oficina 1. 06002 Badajoz, Spain.
[132] J.D. Lawson, Some Criteria for a power producing thermonuclearreactor, (Technical report) (1955), Atomic Energy Research Establishment, Harwell, Berkshire, U.K., A.E.R.E., GP/R 1807.
[133] C. Patrignani, K. Agashe, G. Aielli, C. Amsler, M. Antonelli, D.M. Asner, H. Baer, Sw. Banerjee, R.M. Barnett, T. Basaglia, C.W. Bauer, J.J. Beatty, V.I. Belousov, J. Beringer, S. Bethke, H. Bichsel, O. Biebel, E. Blucher, G. Brooijmans, O. Buchmueller, V. Burkert, M.A. Bychkov, R.N. Cahn, M. Carena, A. Ceccucci, A. Cerri, D. Chakraborty, M.-C. Chen, R.S. Chivukula, K. Copic, G. Cowan et al., (Particle Data Group), *Rev. Particle Phys., Chinese Physics C* **40** (2016)100001.
[134] N. Bohr, *Philosophical Magazine* **26** (6) (1913) 1–25.
[135] Hideki Yukawa, Meson theory in its developments, Nobel Lecture, December 12, 1949.
[136] V. Dubinko, Nuclear catalysis mediated by localized anharmonic vibrations, *Cond-Mat. Mtrl-Sci.* (2015) 1–36. ArXiv: 1510.06081v1. On-line Cornell University Library, Ithaca, NY.
[137] L. de Broglie, The wave nature of the electron, Nobel Lecture, December 12, (1929).
[138] L. Landau and E. Lifchitz, Physique Theorique. Coll. MIR. Ellipses Eds. 1997
[139] P. Grangier, G. Roger and A. Aspect, *Europhys. Lett.* **1** (4) (1986) 173–179.
[140] S. Massidda, Superconductivity Report from BCS to modern electronic theory, University of Cagliari, 2015.
[141] A. Einstein and N. Rosen, The particle problem in the general theory of relativity, *Phys. Rev.* **48**(1935)73.
[142] A.Y. Liu and M.L. Cohen, *Phys. Rev. B* **41** (1990)10727.
[143] E. Schrödinger Erwin, An undulatory theory of the mechanics of atoms and molecules, *Phys. Rev.* **28**(6) (1926) 1049–1070.
[144] J.F. Geneste, Physique de l'esprit des Lois, 951(2010) Cepaduès Editions, Sciences, Toulouse, France, ISBN: 9782854289510.
[145] J.D. Anderson, *Governing Equations of Fluid Dynamics, in Computational Fluid Dynamics*, J.F. Wendt (Ed.), 3rd edition, Springer-Verlag, Berlin, Heidelberg, 2009.
[146] C. Yulksel, PhD Disertation, Real Time Water Waves with Wave Particles, Texas A&M University, 2010.
[147] K. Kunisch and S. Volkwein, Galerkin proper orthogonal decomposition methods for a general equation in fluid dynamics, *SIAM J. Numer. Anal.* **40**(2) (2006) 492–515.